Stability investigation and stabilization of a heavily fractured and loosened rock slope during construction of a strategic hydropower station in China

Tao Chen[a], Jianhui Deng[a,*], Nicholas Sitar[b], Jun Zheng[c], Tiexin Liu[a], Aijuan Liu[a], Lu Zheng[d]

[a] State Key Laboratory of Hydraulics and Mountain River Engineering, College of Water Resource & Hydropower, Sichuan University, Chengdu 610065, China [b] Department of Civil and Environmental Engineering, University of California, Berkeley, CA 94720, USA [c] Department of Civil Engineering, Zhejiang University, Hangzhou 310058, China [d] Institute for Disaster Management and Reconstruction, Sichuan University - Hong Kong Polytechnic University, Chengdu 610065, China

* Corresponding author. E-mail address: jhdeng@scu.edu.cn (J. Deng)

Abstract

This paper presents a case history of the 205 m high intake slope at the Huangjinping (HJP) hydropower station on the Dadu River. Deformation and cracks developed on the cut slope during excavation, and the deformation extended onto the natural slope above the cut, giving rise to serious safety concerns. Research was conducted to study the engineering geological conditions and the deformation characteristics of the slope during excavation. In situ monitoring data and possible causes of cracking were analyzed. The results show that the zone of loosened rock mass extended much deeper into the rock mass than it did at other sites in the region because of the tectonic history of the site and cutting. The empirically designed cable anchors with lengths of 40 m or 45 m were insufficient to stabilize the slope, while the remedial cable anchors as long as 100 m successfully stabilized the slope. The analytic method and procedure used in this paper could be useful to similar projects.

1. Introduction

The Western Sichuan Province is located on the eastern rim of the Tibetan Plateau, and the dramatic change in relief makes it one of the richest hydropower resource districts in China. Over the past 30 years, more than 20 large-scale hydropower projects have been constructed or are under construction along the three major rivers, i.e. the Jinsha River, Yalong River and Dadu River (in Fig. 1). Because of the region's deep down cutting river valleys, active tectonic environment, and weathering processes, rock slope stability has been one of the key engineering problems not only in the studied area, but in several areas worldwide (Qi et al., 2004; Yao et al., 2006; Xu et al., 2011; Song et al., 2011; Tokiwa et al., 2011; Chen et al., 2012; Mineo et al., 2015; Stead and Wolter, 2015). In the studied area, the height

of natural slopes can reach over 1000 m, and cut slopes measuring 300–500 m in height are common. Though various control measures were taken, stability issues did arise from time to time. To the authors' knowledge, most of the stability problems were caused by a lack of recognition during the pre-construction investigation of the persistent discontinuities, such as those in the right abutment slope at Changheba (CHB; Chen et al., 2012), the intake slope at Houziyan (HZY; Fan et al., 2009) and the right abutment slope at Dagangshan (DGS; Li et al., 2014). The objective of this paper is to describe the investigation, analysis, and stabilization of the intake slope of the HJP hydropower station on the left bank of Dadu River, which experienced severe cracking and deformation during construction.

2. Project background

The HJP hydropower station is located in Kangding County, Sichuan Province, China (in Fig. 1). HJP is a clay-core rockfill dam with a maximum height of 95.5 m on Dadu River; it creates a reservoir of 1.28×10^8 m^3 at the normal pool level of 1476.00 m. Two underground powerhouses were built in the left and right abutments. The powerhouse in the left abutment is bigger, with an installed capacity of 800 MW, while the one in the right abutment is smaller, with an installed capacity of only 50 MW. Three intake tunnels were built in the abutment, i.e. the intake tunnels No. 1 and No. 2, and the spillway tunnel (in Fig. 2).

2.1. Engineering geology

The site is located where the Tibetan plateau gradually descends into the Sichuan basin. High mountains and deep cut river valleys are the major geomorphic features in this region. Near the dam site, the Dadu River flows from north to south, and the altitude of the surrounding mountains is typically more than 3000 m above sea level. The highest peaks are 5123 m and 5241 m on the left and right banks, respectively, while the elevation of the river is 1370 m. The Gongga Mountains (GGM) which is the highest mountain in Sichuan province is located in the southwest (in Fig. 1).
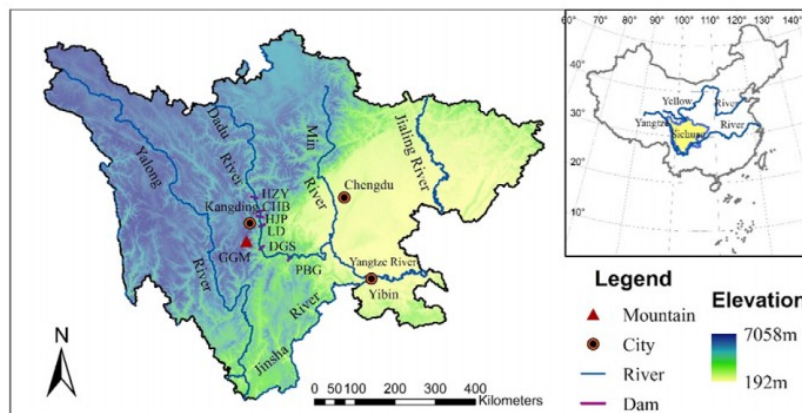

Fig. 1. Geographical location of the HJP hydropower station. GGM = Gongga Mountains; HZY = Houziyan hydropower station; CHB = Changheba hydropower station; HJP = Huangjinping hydropower station; DGS = Dagangshan hydropower station; PBG = Pubugou hydropower station.

The regional tectonic setting is characterized by the three famous fault belts in Western Sichuan Province, which are the NE-SW-trending Longmenshan fault belt (LMF), the NW-SE-trending Xianshuihe fault belt (XSF), and the N-S-trending Anninghe fault belt (ANF) (in Fig. 3). All three fault belts are active, and epicenters of historical earthquakes for the region are plotted in Fig. 3. The most recent significant earthquakes in the region were the Wenchuan earthquake (Mw = 7.9) on May 12, 2008, and the Lushan earthquake (Mw = 6.6) on April 20, 2013. The seismicity of the study area is highly due to its proximity to active fault belts.

The climate in the region is semitropical and monsoonal, but the Dadu River valley is hot and dry. Statistical data from the Luding Meteorological Station indicates that the yearly average temperature is 15.4 °C, with a high of 34.4 °C and low of −5.0 °C. In the river valley, the air is quite dry, and evaporation significantly exceeds the precipitation. Yearly average precipitation is only 634.9 mm, while the evaporation potential can reach 1532 mm. The period from May to October is the rainy season, with about 90% of the yearly precipitation. In this period, June, July and August are the rainiest months, with more than 64% of the total precipitation.
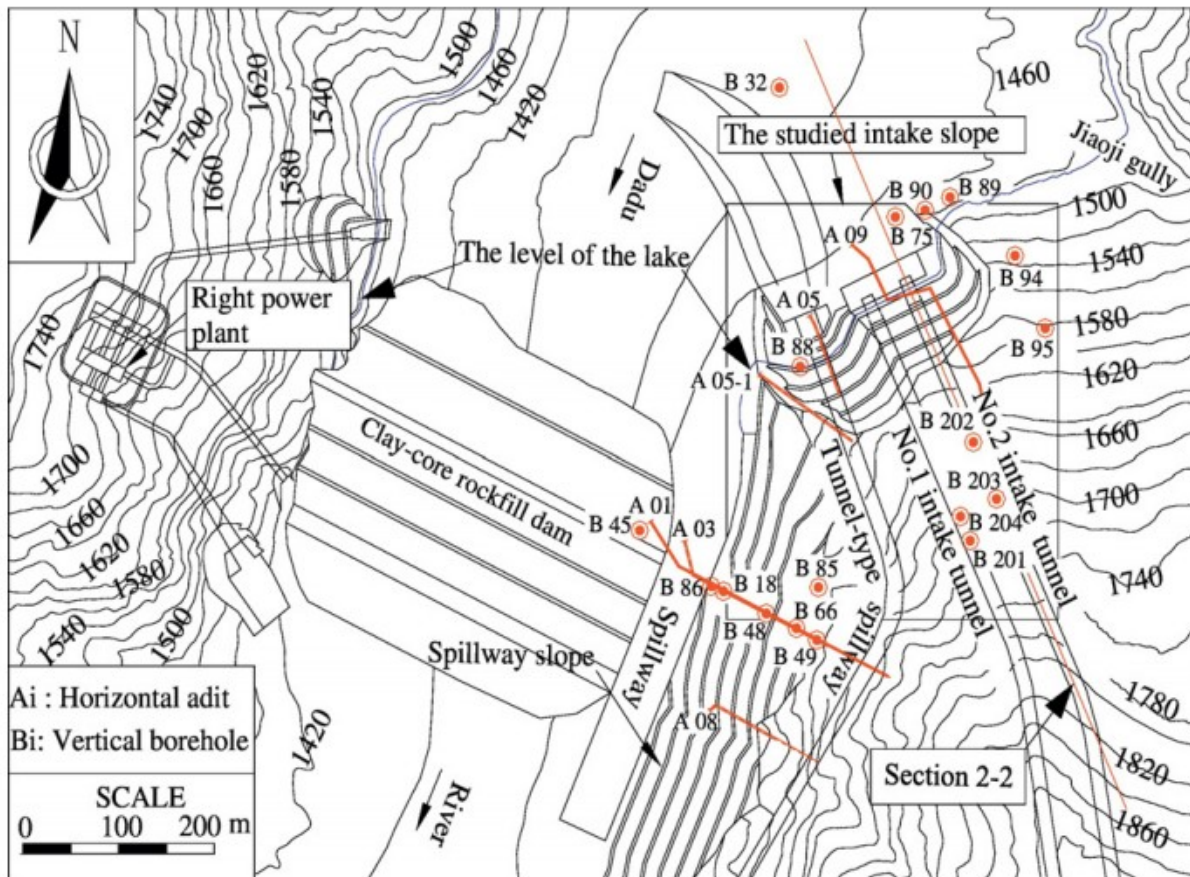

Fig. 2. Plan view of the HJP hydropower station.

Bedrock at the site is composed mainly of plagioclase granite and quartz diorite of the Kangding complex, belonging to the lower Proterozoic metamorphic complex and Jingning-Chengjiang magmatic complex (Zu and Jiang, 1988; Chen et al., 2005), which are widely distributed in the area bounded by the three fault belts. Subsequent to formation, these rocks have been altered and deformed by a series of successive tectonic events, including the Caledonian movement, Hercynian movement, Indosinian movement, Yanshan movement and Himalaya orogeny, which have thus created very complex structures.
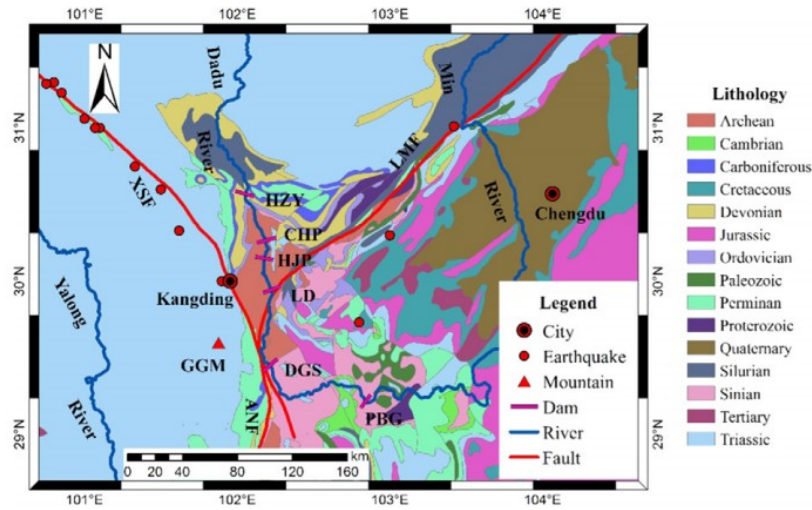

Fig. 3. Geological map of HJP site and the epicenters of famous historical earthquakes. XSF = Xianshuihe fault belt; ANF = Anninghe fault belt; LMF = Longmenshan fault belt; GGM = Gongga Mountains; HZY = Houziyan hydropower station; CHB = Changheba hydropower station; HJP = Huangjinping hydropower station; DGS = Dagangshan hydropower station; PBG = Pubugou hydropower station.
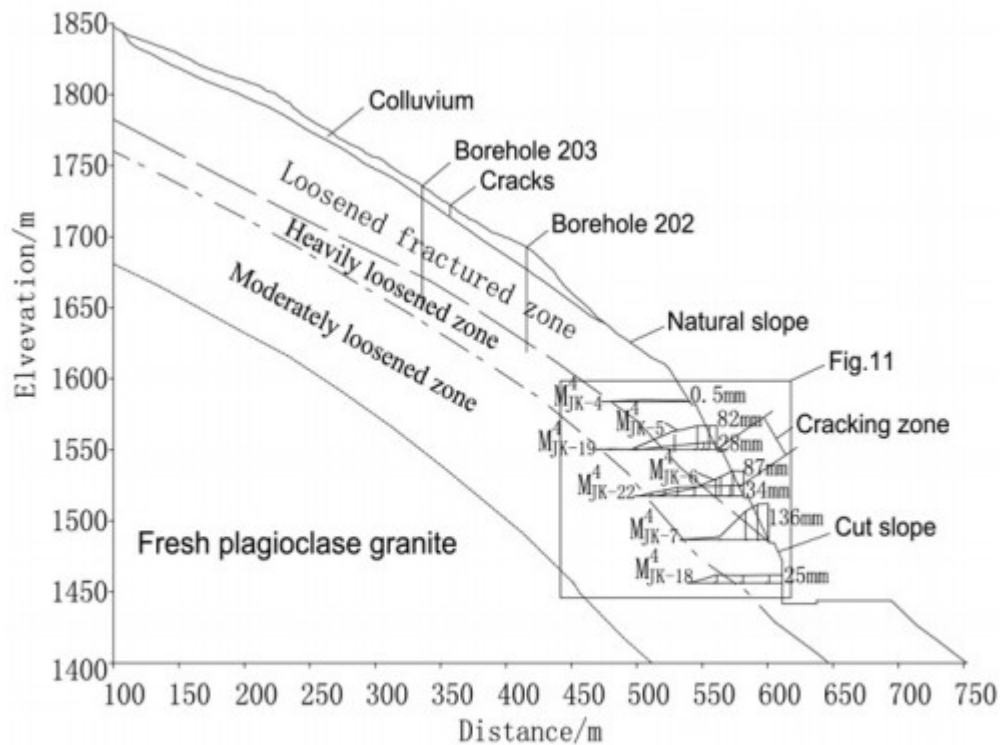
Fig. 4. Identification of different zones of section 2-2, with respect to the fracturing condition of the rock.

Abundant geological prospecting work was done at the site. Vertical boreholes and horizontal adits are displayed in Fig. 2. The investigation indicates that the rock mass of the intake slope has been extensively fractured and jointed. The degree of fracturing and jointing increases toward the ground surface, resulting in an increasingly loosened rock mass. As shown schematically in the cross section (in Fig. 4), the loosened fractured zone extends to a depth of about 50 m, and the entire zone of loosened rock mass reaches to approximately 150 m below the ground surface. The heavily loosened rock mass is usually mildly weathered, with a fractured surface layer. The drill core of loosened fractured zone is fragmental with tiny short column (in Fig. 5(a)), while that of heavily loosened zone is relatively intact (in Fig. 5(b)). The rock mass along slopes above the river banks is extensively fractured and highly permeable (in Fig. 6). Stable groundwater levels were not found during pre-construction investigations.

Fig. 5. The drill core of: (a) loosened fractured zone (b) heavily loosened zone.

Fig. 6. The fractured and highly permeable rock mass.

2.2. Design of the left abutment intake slope

The left abutment intake slope is comprised of two parts, the cut and the natural slope. The cut slope starts at elevation 1620 m and ends at elevation

1415 m (the base of the tunnel spillway), which maximum height is 205 m. A slope ratio of 1:0.5 was adopted for all benches on the cut slope, except for the lowest bench, which was vertical (Figs. 4 and 11). Benches were set vertically every 30 m and were usually 3 m wide. The natural slope above the cut slope has a height of over 500 m with an angle of 40–50°.

The designed slope protection and reinforcement scheme consisted of three elements. First, 5 cm of shotcrete was applied to all newly excavated surfaces, and welded mesh was added wherever the rock mass was heavily weathered or the local colluvium layer was removed. Second, rock bolts, arranged at intervals of 1.5 m, were used for shallow support, with the bolt length varying from 4.5 to 9.0 m. Third, cables were used to control the deformation and stability of the slope. In general, the cables were to be used with a reinforced concrete lattice with a spacing of 5 × 5 m, except where the rock mass was comparative blocky. The designed capacity of the cables was 1500–2000 kN, with a length of 30–45 m at elevations from 1620 m to 1481 m, 55–60 m at elevations from 1481 m to 1415 m, respectively (Hydrochina Chengdu Engineering Corporation, 2012).

2.3. Layout of monitoring instruments

In September 2011, ten geodetic points (TP01-TP10) were installed on the natural slope. In November 2011, nineteen geodetic points (TP$_{JK01}$-TP$_{JK19}$) were installed on or near the cut slope. The locations of these points are shown in Fig. 7.

In order to monitor the rock mass deformation, from January 2011 to October 2011, sixteen multipoint extensometers (M$^4_{JK-1}$-M$^4_{JK-16}$) were installed in four sections (in Fig. 8). However, some multipoint extensometers were destroyed by follow-up construction; these were replaced with new multipoint extensometers installed in the same positions. Meanwhile, as illustrated in Fig. 8, load cells for the cables were installed in four sections on the cut slope. Inclinometer casings for detecting potential slip planes were installed in the boreholes. After the large deformation, twelve inclinometers were installed to monitor the further deformation and potential slid surface.

3. Observations during excavation and analysis of monitoring data

3.1. Observations during excavation

Excavation began in June 2010. During the first year, excavation went smoothly, although the reinforcing work was slightly delayed. In August 2011 (line 1 in Fig. 10), the excavation was down to elevation 1482 m, and extension cracks were first noticed in the natural slope (Crack A in Figs. 7 and 9(a)). Excavation was therefore forced to cease from August 2011 to October 2011. In September 2011 (line 2 in Fig. 10), cracks were observed in the cut slope between benches at 1510 and 1540 m (Cracks B and C in Figs. 7 and 9). Although reinforcing work was expedited, the deformation continued. In November 2011 (line 3 in Fig. 10) the extension cracks in the natural slope extended, and a persistent, armchair-shaped crack was

formed. Despite the ongoing deformation, excavation resumed. In December 2011 (line 4 in Fig. 10), even though the installation of the designed cable anchors was mostly complete, the deformation continued. The tensile cracks in the natural slope were still expanding rapidly, and numerous new cracks appeared in the cut slope between elevation 1570 and elevation 1580 m. Some lattice beams also fractured in that zone (Crack D in Figs. 7 and 9(d)). By the end of February 2012, the maximum horizontal displacement of the fractures on the natural slope reached 231 mm, and the maximum vertical settlement displacement was 150 mm. The deformation was brought about under control only when supplementary reinforcement was installed in June 2012 (in Fig. 10).

3.2. Analysis of monitoring data

The deformation vectors for the entire intake slope, as plotted in Fig. 7, indicate that the whole slope was deformed to the northwest. Although the installation of multipoint extensometers lagged behind excavation, the extensometer results still indicate that the excavation had an obvious influence on the deformation. A typical curve of deformation-time is shown in Fig. 10. For M^4_{JK-7}, just during the excavation from elevation 1460 m to elevation 1415 m. Fig. 11 shows a typical curve of deformation-horizontal depth at cross section 2-2. The results indicate that the maximum depth of deformation was around 65 m, which is roughly the horizontal distance to the base of the heavily loosened zone. Fig. 11 also shows that the largest deformation occurred above elevation 1481 m, i.e. the elevation at the outcrop of the loosened fractured layer in the cut slope. Therefore, the major deformed body was the loosened fractured zone, and the depth of which was beyond the designed cable length of 60 m. As a result, the designed cable bolts had a limited capacity to control deep deformation, and the deformation of the natural slope was the result of structural adjustments of loosened fractured zone. In addition, curves of deformation - horizontal depth (in Fig. 11) indicate that the deformation characteristics of the slope were similar to those of particles. And there were no preferred structural planes, which have a significant influence on the deformation.

Concurrent with the additional instrumentation, the locked-in load of the installed cable anchors was monitored (in Table 1). The data show that by January 3, 2014, the average loss rate of the locked tonnage was 11%. Five cable anchors lost more than 10% of their initial locked-in load, with a maximum loss of 64% for cable PR_{JK-14}. This loss of load persisted, even after a second round of grouting, due to the heavily fractured and loosened rock mass. The deformation patterns in the extensometer data indicate that the designed cable anchors functioned only to lock part of the loosened fractured rock mass, making the bolted surface of the cut slope behave essentially as a retaining wall.
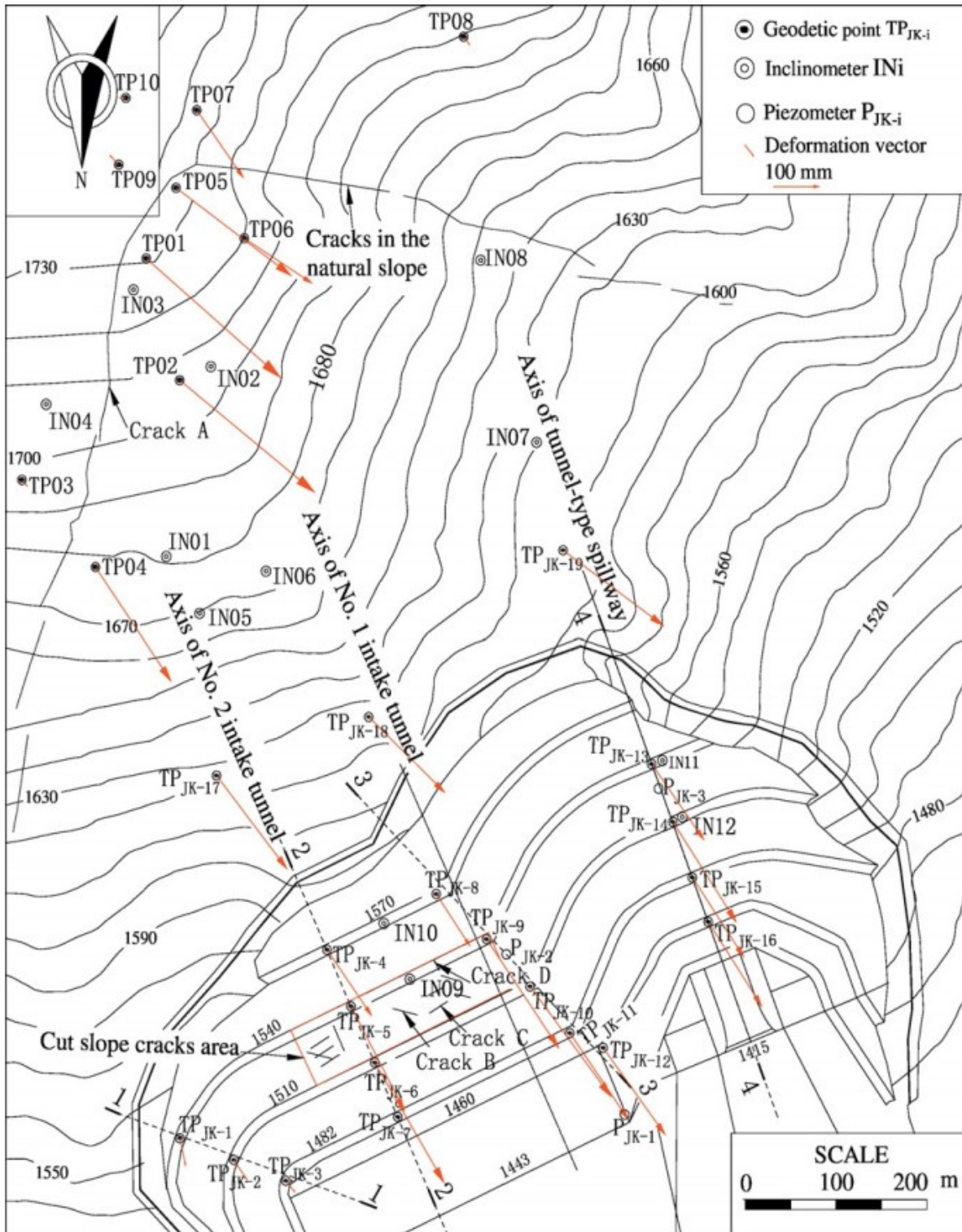
Fig. 7. Cracks and deformation vectors of the intake slope. Note: digital photos of cracks A – D are shown in Fig. 9.

3.3. Removable infinite blocks in cut slope cracking area

The principal idea behind block theory analysis (Goodman and Shi, 1985) is that it allows many different combinations of discontinuities to be passed over, and it allows for the direct identification and consideration of critical rock blocks known as "key blocks". Fig. 12 shows five types of blocks in a surface excavation formed by discontinuities. Although the actual blocks exist in three dimensions, to simplify the illustration, a two-dimensional figure is used (Um and Kulatilake, 2001; Liu et al., 2017). According to Fig. 12, type (a) is an infinite block that is incapable of internal cracking, and is therefore not dangerous; type (b) is a finite block that is non-removable because it is tapered by adjacent blocks; type (c) is a stable block, without friction, under gravity alone; and type (d) can remain stable only under gravitational loading. However, it can come out into the free surface of excavation if there are external forces like water forces, inertia forces, etc. Therefore, a type (d) block is a potential key block. Finally, a type (e) block can slide into free space under gravitational loading without any external force unless a proper support system is provided. Therefore, type (e) is a key block.

Field investigations showed a diabase vein (βμ6) and three sets of discontinuities (L1, L2, and L3) in the cut slope cracks area. The mean orientations of those discontinuities are listed in Table 2. Block theory analysis of the joint data identified two removed infinite blocks: block 0000 and block 1100, as shown in Fig. 13. Worse still, the reinforced concrete lattice was not used in this area, because the rock mass in the zone had more widely spaced joints. Therefore, the cracking was most likely caused by the moving of the key blocks, i.e., the deformation was localized in the zone without lattice support.

4. Local tectonic uplift and influence on geologic framework of the HJP intake slope

4.1. The uplift of Gongga Mountains

The Gongga Mountains (GGM), just 61 km away from HJP are the highest mountains near the Dadu River hydropower projects. The present uplift rate of the Gongga Mountains is at least 5.8 mm/yr relative to the Sichuan basin, and it is also not less than 3.0–4.0 mm/yr relative to the Anning River valley. This rate is comparable with the uplift of the Himalaya Mountains (Wang et al., 2008). In the following section, we will discuss the influence of the uplift on the geologic framework, including the depth of loosened rock mass, the in-situ stress and the distribution of discontinuities.
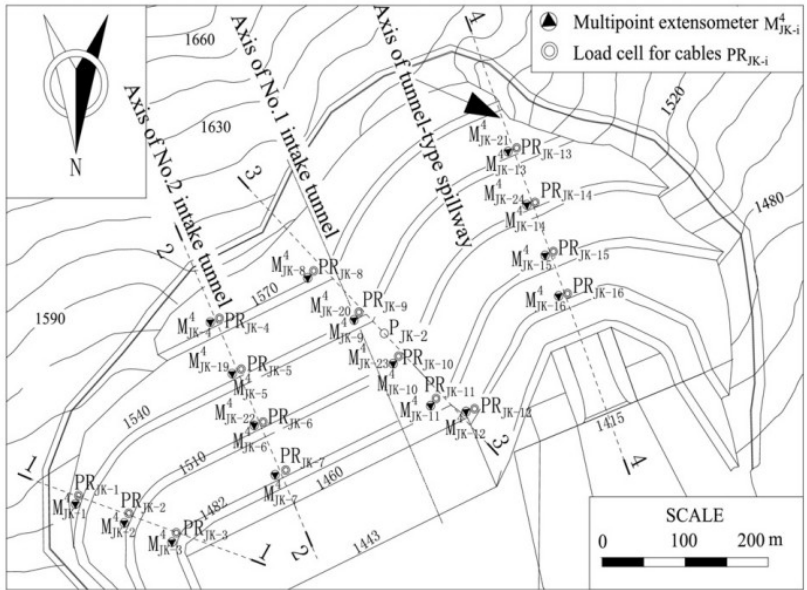
Fig. 8. Monitoring instruments on the cut slope. Note: M^4_{JK-1} to M^4_{JK-16} were destroyed by follow-up construction, and M^4_{JK-1} - M^4_{JK-16} were installed at the same position to replace them.

(a) Crack A on the natural slope.

(b) Crack B on the cut slope.

(c) Crack C on the cut slope.

(d) Crack D on reinforced concrete lattice

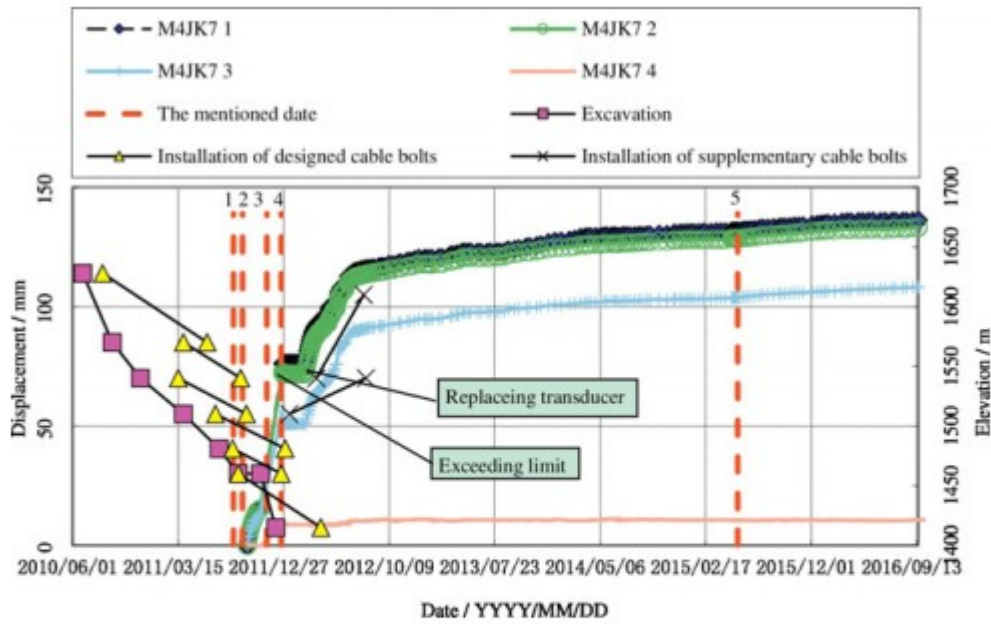**Fig. 9.** Cracks on the intake slope.

Fig. 10. Displacement vs excavation and reinforcement. Note: M4JK-7 is a multipoint extensometer, the depth of points 1, 2, 3, 4 is 0 m, 10 m, 54 m, 62 m respectively; the red dotted lines 1–5 are the important dates mentioned in this paper. (For interpretation of the references to color in this figure legend, the reader is referred to the web version of this article.)
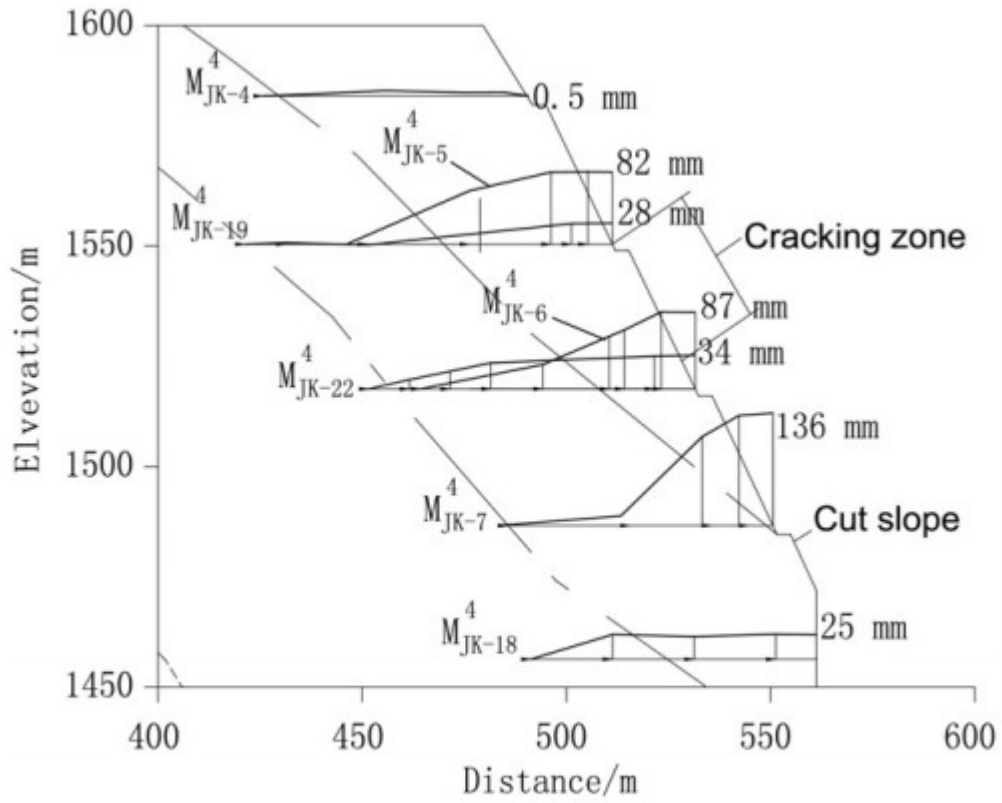
Fig. 11. Deformation-horizontal depth curves of section 2-2. Note: Displacement unit is mm; M^4_{JK-4} is unavailable.

(a) infinite
(b) finite
    nonremovable,
    tapered
(c) finite, removable,
    stable without
    friction
(d) finite, removable,
    stable with
    sufficient friction
(e) finite, removable,
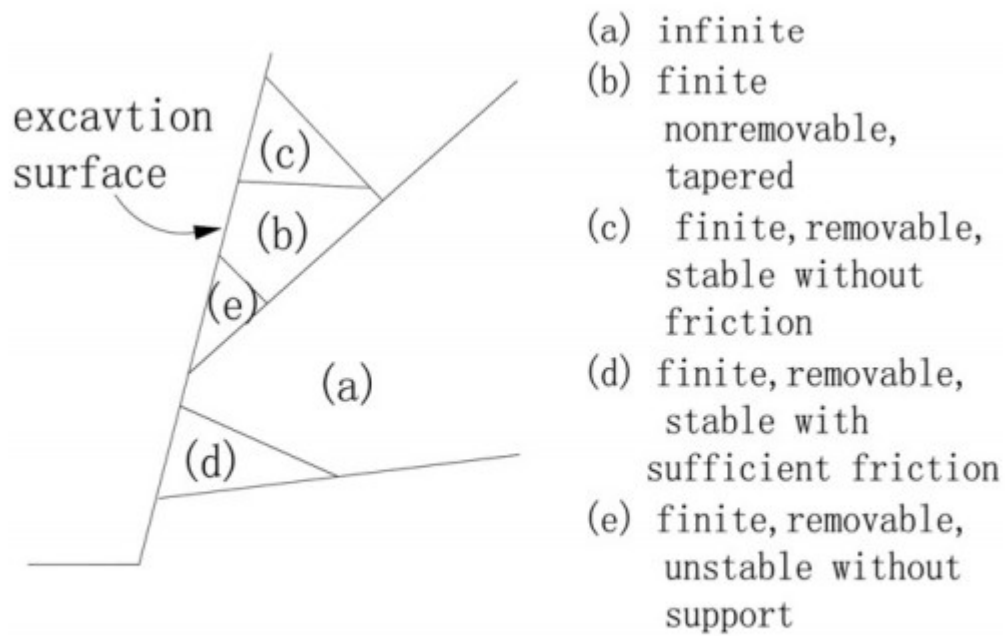   unstable without
    support

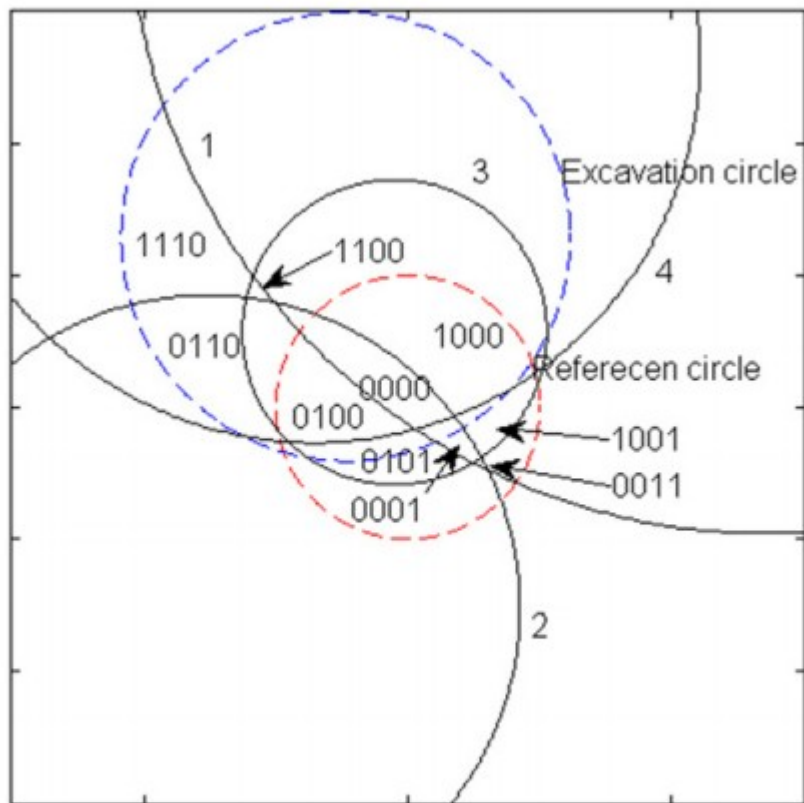**Fig. 12.** Blocks in a surface cut (Um and Kulatilake, 2001).

Fig. 13. Identification of removable blocks for cut slope cracking area using stereographic projection. Note: block 0000 and block 1100 are removable infinite blocks.

Table 1
Monitoring results of initially designed cable bolts.

#	Elevation/m	First date/YYYY/MM/DD	Last date/YYYY/MM/DD	Locked value/kN	Last value/kN	Loss rate/%
PR_{JK-1}	1540	2011/05/15	2012/12/17	1657.42	1459.00	12
PR_{JK-2}	1512	2011/08/25	2014/01/03	1650.32	1679.83	−2
PR_{JK-3}	1482	2012/02/10	2014/01/03	2150.30	1966.66	9
PR_{JK-4}	1572	2011/04/02	2014/01/03	2160.31	2006.00	7
PR_{JK-5}	1542	2011/05/27	2014/01/03	2229.94	2179.82	2
PR_{JK-6}	1512	2011/06/22	2014/01/03	1666.56	1577.28	5
PR_{JK-7}	1482	2011/12/09	2014/01/03	2203.41	2326.73	−6
PR_{JK-8}	1572	2011/03/29	2014/01/03	2186.45	1941.10	11
PR_{JK-9}	1542	2011/05/28	2014/01/03	2243.45	2063.35	8
PR_{JK-10}	1543	2011/11/30	2014/01/03	1647.12	1621.00	2
PR_{JK-11}	1482	2011/10/26	2013/09/06	2188.05	1293.21	41
PR_{JK-12}	1462	2011/12/17	2012/11/10	1639.86	1368.21	17
PR_{JK-13}	1545	2011/06/09	2014/01/03	1677.49	1597.13	5
PR_{JK-14}	1510	2011/07/04	2014/01/03	2209.00	794.36	64
PR_{JK-15}	1511	2011/10/25	2014/01/03	2106.90	2242.73	−6
PR_{JK-16}	1462	2011/12/10	2014/01/03	1657.92	1579.52	5

Table 2

Mean orientations of main discontinuity sets in the cracking zone of the cut slope.

Discontinuity	β_{u6} (1)	L1 (2)	L2 (3)	L3 (4)	Excavation face
Dip angle/°	78	65	30	70	54
Dip direction/°	35	225	350	345	340

Table 3

In-situ stress and horizontal loosened depth on slopes at adjacent hydropower projects along the Dadu River and their linear distance from the Gongga Mountains.

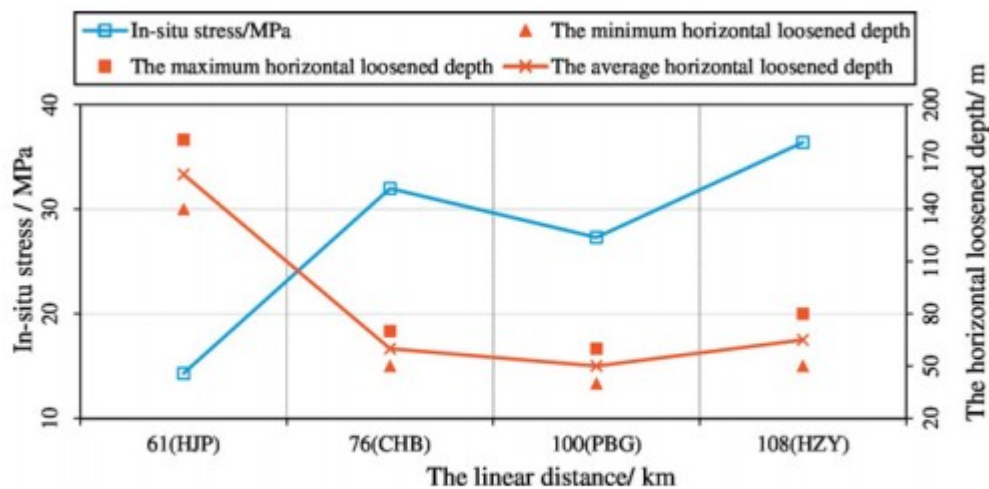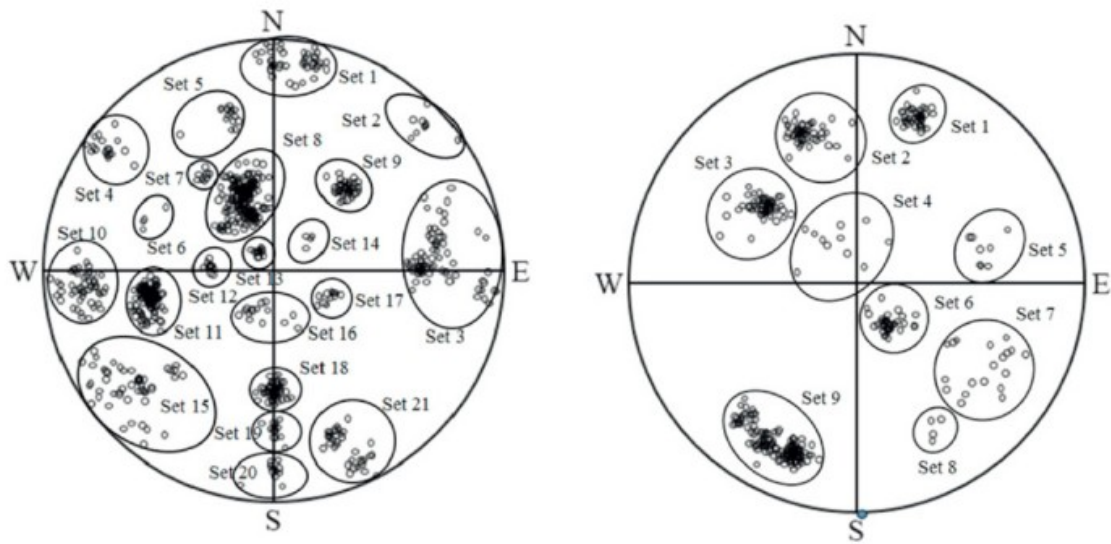| Serial no.	Project name	Linear distance to Gongga Mtn/km	First principal stress/MPa	Horizontal loosened depth/m	Slope dip angle/°
1	HJP	61	14.3	140–180	43–74
2	CHB	76	32.0	50–70	40–60
3	PUG	100	27.3	40–60	40–60
4	HZY	108	36.4	50–80	40–65

Fig. 14. In-situ stress and horizontal loosened depth vs linear distance from the Gongga Mountains.

(a) HJP intake slope

(b) CHB right abutment slope.

Fig. 15. Orientation distribution of normal discontinuity vectors.
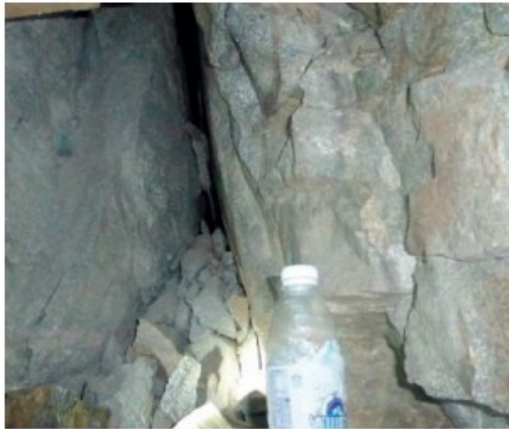
(b) The horizontal depth is 130m

(c) The horizontal depth is 170m.

Fig. 16. Typical open joints in the loosened rock mass on the HJP intake slope.
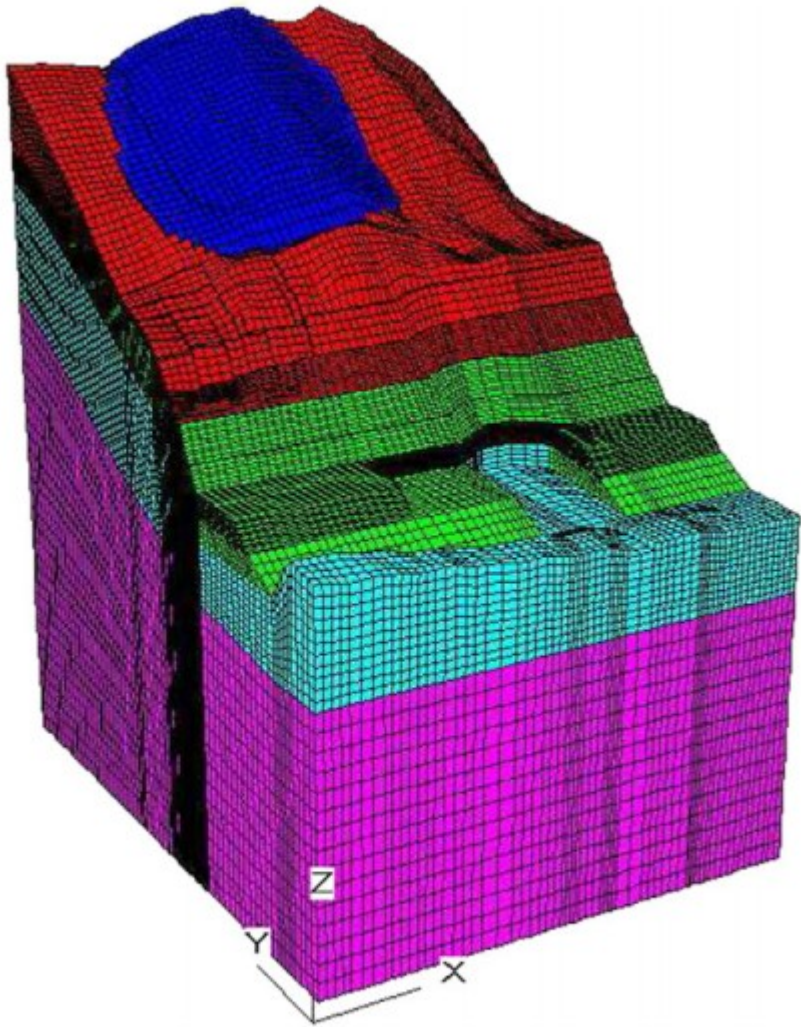
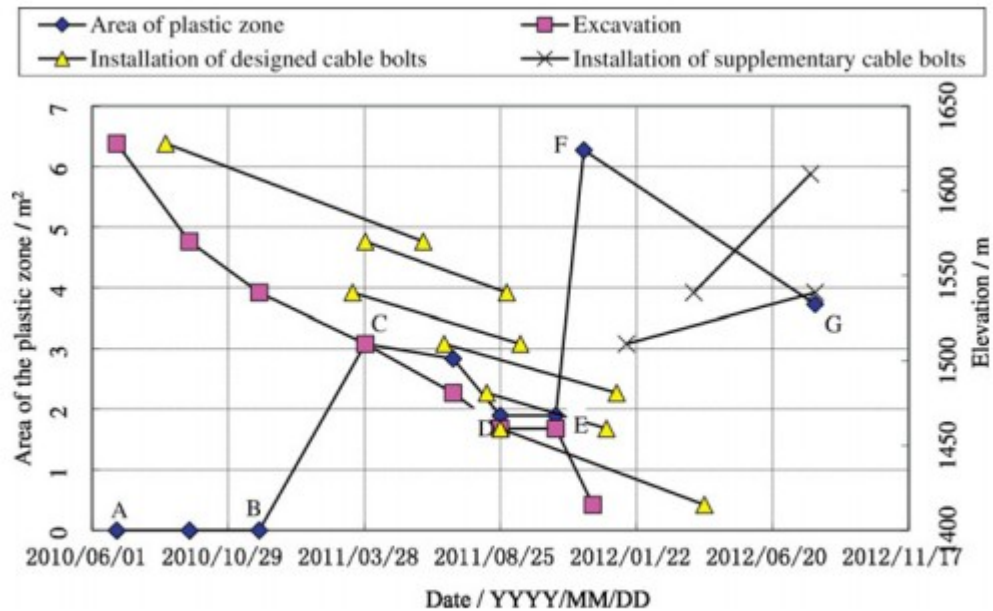**Fig. 17.** 3D mesh for FDM modeling (after excavation).

Fig. 18. The plastic zone process during excavation.

4.2. The influence on geologic framework

In Table 3, the authors has summarized the maximum in-situ stress at the underground powerhouse, and the horizontal loosened depth of the bank slopes of four hydropower projects on the Dadu River. Then, the relationship between the above results and the distance from the Gongga Mountains (GGM) are drawn in Fig. 14. These comparisons indicate that the closer the site to the Gongga Mountains (GGM), the lower the in-situ stress magnitude and the larger the horizontal loosened depth. Among the four projects, the horizontal depth of the loosened zone is the greatest at the HJP project site, while the measured maximum in-situ stress is the lowest. Second, in order to study the influence on the rock mass structure, the authors compared the distribution of discontinuities between the left abutment intake slope of the HJP and the right abutment slope of CHB, which is somewhat far from the Gongga Mountains. For the HJP intake slope, 733 discontinuities divided into 21 sets were mapped, as shown in Fig. 15(a). For the right abutment slope of CHP, only 341 discontinuities divided into 9 sets were mapped, as shown in Fig. 15(b). These results indicate that the discontinuities on the HJP intake slope are abundant and essential; no persistent and dominating discontinuity trends were identified. In addition, the joints and fractures remained open, and did not progressively close with depth, as would be expected with increasing overburden stress (in Fig. 16).

4.3. Discussion

The rock mass of the HJP intake slope was found far more loosened and fractured than that observed at adjacent projects, with the characteristic that is closely related to the uplift of the Gongga mountains. An additional

factor leading to the relaxation of the rock mass is the rapid down cutting caused by the river. Because the HJP site is relatively close to the fast-uplifting Gongga mountains, the down cutting rate is faster, which leads to faster stress drop and greater dilation of the rock mass. The result is a greater relaxation depth or thicker loosened zone.

Additionally, the persistent tectonic uplift produced open joints and fractures that were later intruded by magma and re-welded. This process was repeated during past tectonic epochs, and the presently exposed rock is quite similar in appearance to a stone-rich concrete. This special rock mass is called the Kangding complex; it is the major rock mass in the HJP intake slope and is widely distributed nearby.

The special geologic framework of the HJP intake slope is influenced by a combination of local uplift and river down cutting. This framework is the essential cause of the slope's deformation characteristics, which include sensitivity to excavation disturbance, deep deformation and particle-like performance, as discussed above. In addition, this understanding is helpful in the design of mitigation measures.

5. The mitigation measures and effect verification

5.1. Mitigation measures

Based on the above analysis, remedial measures using conventional rock mass stabilization measures were considered feasible, and cable anchors offered the most optimal means for reinforcement. Consequently, the design parameters of the remedial cable anchors were adjusted as follows: first, the length of the as-yet uninstalled cable anchors at elevations between 1481 and 1510 m were increased to 70 m or 75 m, up from the initial 40 m or 45 m. After January 11, 2012, these lengths were further extended to 100 m, in order to provide anchorage beyond the zone of significant loosening of the rock mass. Second, new cable anchors were added from elevation 1510 m to elevation 1610 m, on a 4 × 4 m grid with an installed capacity of 2500 kN or 3000 kN. The installation of cable anchors was carried out in two phases. The first phase took place at elevation 1510–1540 m, and the second phase took place at elevations 1540–1610 m.

5.2. Numerical analysis

5.2.1. Analysis method and model

The purpose of the numerical analysis is to evaluate slope stability after the installation of remedial measures. As no dominating discontinuities were recognized as well as the deformation characteristics were similar to those of particles, the slope rock mass was modeled as a continuous material. 3D Fast Lagrangian Analysis of Continua (FLAC^{3D}) was used to perform the analysis (Itasca, F. L. A. C., 2000). The model geometry and mesh are shown in Fig. 17.

Table 4
Physical and mechanical parameters for the rock mass of the HJP intake slope.

Material	Constitutive relation	Yield criterion	Density/g/cm^3	Young's modulus/GPa	Poisson's ratio	Tensile strength/MPa	Shearing strength $\phi'/°$	c'/MPa
Colluvium	Perfect-plasticity	Mohr-Coulomb	2.00	0.8	0.40	0	30	0.03
Loosened and fractured zone	Perfect-plasticity	Mohr-Coulomb	2.50	1	0.35	0.1	32	0.20
Heavily loosened zone	Perfect-plasticity	Mohr-Coulomb	2.60	3	0.30	0.5	34	0.40
Moderately loosened zone	Perfect-plasticity	Mohr-Coulomb	2.60	6	0.29	1.0	39	0.70
Fresh plagioclase granite	Linear elasticity	–	2.60	12	0.24	1.5	47	1.10

Because the fresh and unloosened rock mass was far beyond the excavation disturbance range, a linearly elastic model was adopted for the numerical analysis. The other portions rock mass, including colluviums, loosened fractured zone, heavily loosened zone and moderately loosened zone was modeled as perfectly plastic material, and a Mohr-Coulomb model was used. The material parameters used in the modeling (in Table 4) are based on the numerous field and laboratory tests conducted by the designing institute. A three-dimensional (3-D) strength reduction technique (Dawson et al., 1999; Deng et al., 2007; Wei et al., 2009) was used to obtain the safety factors of the slope under various conditions. The critical state was assumed to occur when a continuous plastic band formed.
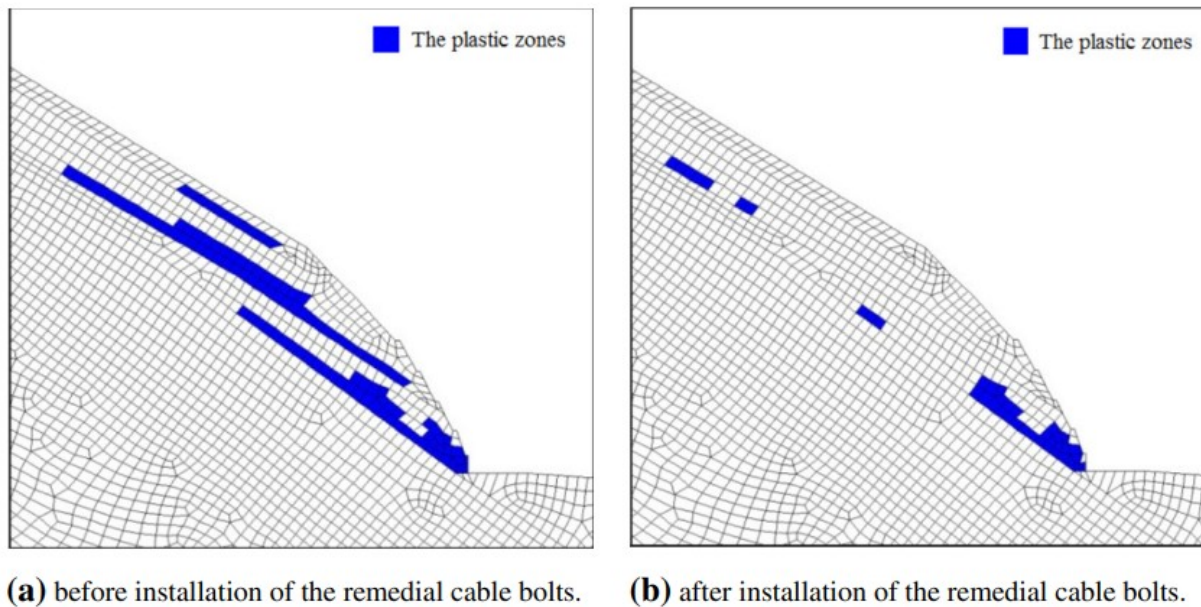

(a) before installation of the remedial cable bolts. **(b)** after installation of the remedial cable bolts.

Fig. 19. Comparison of the extent of the plastic zones in section 2-2.

5.2.2. Analysis results

The construction process, including excavation and the installation of reinforcements, was simulated according to the actual work performed on the slope. The area of the plastic zone in key sections, such as section 2-2, was calculated using the FISH program. The process of extent of plastic zone during excavation (in Fig. 18) could be divided into six stages. In stage 1 (from point A to B in Fig. 18), because the excavation scope was small, no

plastic zone formed. In stage 2 (from point B to C in Fig. 18), the area of the plastic zone increased rapidly, because of the excavation from 1540 to 1510 m, and the delay in the installation of supporting measures. In stage 3 (from point C to D in Fig. 18) the area of the plastic zone obviously decreased, due to the installation of cable anchors from elevation1570 m to elevation 1482 m. During stage 4 (from point D to E in Fig. 18), excavation had to be suspended because of the large deformation of the slope. In stage 5 (from point E to F in Fig. 18), because of the vertical excavation below elevation 1460 m, the plastic zone once again increased rapidly. In this stage, a persistent, armchair-shaped crack formed on the natural slope. These phenomena indicate that the numerical results are consistent with slope observations taken during excavation, and that the numerical results are therefore reliable.

As shown in Fig. 18, during stage 6 (from point E to F), the plastic zone was sharply reduced as a result of the installation of the remedial cable anchors. In addition, Fig. 19 shows a comparison of the plastic zones in section 2-2 before and after the installation of the remedial cable anchors. These results also show that the extent of the plastic zone was dramatically reduced after the installation of the remedial reinforcements. The conventionally computed static factors of safety are 1.20 and 1.09 under normal and seismic conditions, respectively. These factors of safety meet the design code requirements, in this case the 2007 Professional Standards of People's Republic of China.
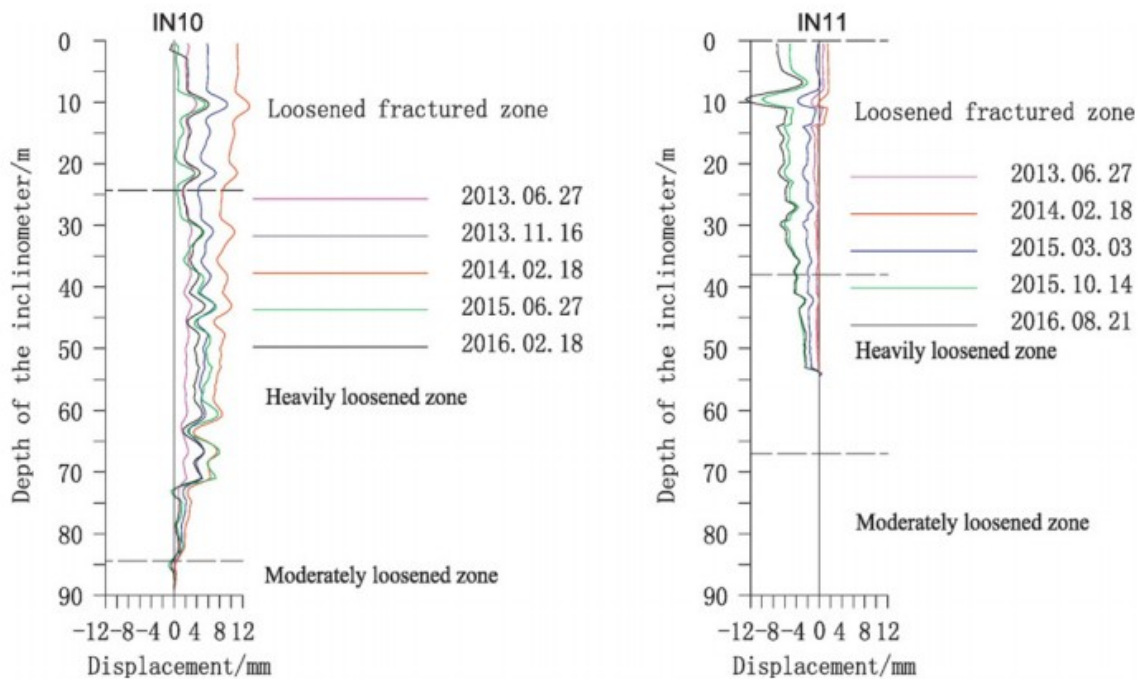

Fig. 20. Results from inclinometers IN10 and IN11.

Table 5
Monitoring results of remedial cable anchors.

#	Elevation/m	First date/YYYY/MM/DD	Last date/YYYY/MM/DD	Locked value/kN	Last value/kN	Loss rate/%
PR_{JK-17}	1600	2012/04/10	2014/01/03	2798.64	2537.57	9
PR_{JK-18}	1585	2012/04/01	2014/01/03	3316.12	3013.18	9
PR_{JK-19}	1575	2012/03/31	2014/01/03	1602.51	1398.50	13
PR_{JK-20}	1541	2012/03/06	2014/01/03	3275.23	3025.84	8
PR_{JK-21}	1458	2012/04/07	2014/01/03	2381.31	2425.50	−2
PR_{JK-22}	1453	2012/02/27	2014/01/03	2173.98	1732.95	20
PR_{JK-23}	1471	2012/06/08	2014/01/03	2166.90	2122.95	2
PR_{JK-24}	1471	2012/03/02	2014/01/03	2511.70	2425.63	3
PR_{JK-25}	1468	2012/06/07	2014/01/03	2405.60	2287.77	5
PR_{JK-26}	1556	2012/07/02	2014/01/03	3334.30	3169.49	5
PR_{JK-27}	1551	2012/08/02	2014/01/03	3281.44	3105.68	5
PR_{JK-28}	1549	2012/08/03	2014/01/03	3289.68	3105.18	6

5.3. Monitoring data verification

After the installation of the remedial reinforcements at the end of June 2012, the stability of the slope greatly improved. First, the deformation detected by the multipoint extensometers tended to converge after the first and second applications of the supplementary cable anchors. Since 2016, the deformation has been just 0.09 mm/month. The deformation can, essentially, be considered to be stopped. Second, no shear deformation was detected by the inclinometers from April 2013 to August 2016 (Fig. 20) and the measured displacements were within the error limit of the instruments. Third, as shown in Table 5, the remedial cable anchors generally experienced relatively minor relaxation—usually less than 10%, with an average value of 7% and a high of 20%.

The final configuration of the HJP intake slope is shown in Fig. 21. The project began impounding water on May 15, 2015 (line 5 in Fig. 10), the first turbine began generating power on September 3, 2015, and the slope is performing well.

Fig. 21. Overall view of the HJP intake slope after completion.

6. Conclusions

This paper presents a history case of the stabilization of a very high and steep rock slope in a highly jointed and fractured rock mass. In this case, a zone of highly loosened rock mass extended well beyond the depth of similar rocks in the same region. These unique conditions were not appropriately recognized during initial investigation. So the effects of empirically designed cable anchors are limited and the slope instability occurred. A comparison with adjacent projects indicates that local uplift has a significant influence on the site's geologic framework. The results of extensive additional investigation indicate that the rock mass did not exhibit any major through-going discontinuities, and could therefore be treated by reinforcement with deep cable anchors extending beyond the zone of loosening. Consequently, the slope stabilization measures included the installation of an extensive grid of cable anchors up to 100 m in length, and the slope was successfully stabilized.

Through this case study, it can be seen that, for this kind of rock mass, attention should be paid to the special rock mass structure, and cable anchors should be long enough to reach the weakly loosened zone. In addition, the analytic method and procedure described in this paper could prove helpful for similar projects.

References

Chen, Y., Luo, Z., Zhao, J., Li, Z., Zhang, H., Song, B., 2005. Petrogenesis and dating of the Kangding complex, Sichuan Province. Sci. China Ser. D Earth Sci. 48 (5), 622–634.

Chen, J., Deng, J., Wei, J., Zhang, A., 2012. Cause analysis of cracking in right abutement slope of Changheba Hydropower Station. Chin. J. Rock Mech. Eng. 31 (6), 1121–1127 (In Chinese).

Hydrochina Chengdu Engineering Corporation, 2012. Stability evaluation and treatment scheme report of diversion tunnel, spillway tunnel entrance slope of Huangjinping hydropower project. Hydrochina Chengdu Engineering Corporation, Dadu River in Sichuan Province (In Chinese).

Dawson, E.M., Roth, W.H., Drescher, A., 1999. Slope stability analysis by strength reduction. Geotechnique 49 (6), 835–840.

Deng, J., Tham, L.G., Lee, C.F., Yang, Z., 2007. Three-dimensional stability evaluation of a preexisting landslide with multiple sliding directions by the strength-reduction technique. Can. Geotech. J. 44 (3), 343–354.

Fan, Y., Wu, F., Wang, G., Zhang, Y., Jiao, T., 2009. Study on stability of the tunnel-face slope at Houziyan Hydropower Station. Chin. J. Geol. Hazard Control 20 (3), 0035–0039 (In Chinese).

Goodman, R.E., Shi, G.-H., 1985. Block Theory and its Application to Rock Engineering. Prentice-Hall Inc., New Jersey.

Itasca, F.L.A.C., 2000. Fast Lagrangian Analysis of Continua. Itasca Consulting Group Inc., Minneapolis, Minn.

Li, M., Wei, W., Zhang, G., 2014. Stability evaluation and reinforcement of unloading fissures in right bank of Dagangshan Hydropower Station. Chin. J. Rock Mech. Eng. 33 (11), 2276–2282 (In Chinese).

Liu, T., Deng, J., Zheng, J., Zheng, L., Zhang, Z., Zheng, H., 2017. A new semi-deterministic block theory method with digital photogrammetry for stability analysis of a high rock slope in China. Eng. Geol. 216, 76–89.

Mineo, S., Pappalardo, G., Rapisarda, F., Cubito, A., Di Maria, G., 2015. Integrated geostructural, seismic and infrared thermography surveys for the study of an unstable rock slope in the Peloritani Chain (NE Sicily). Eng. Geol. 195, 225–235.

Qi, S., Wu, F., Yan, F., Lan, H., 2004. Mechanism of deep cracks in the left bank slope of Jinping first stage hydropower station. Eng. Geol. 73, 129–144.

Song, S., Feng, X., Xiang, B., Xing, W., Zeng, Y., 2011. Research on key technologies for high and steep rock slopes of hydropower engineering in Southwest China. Chin. J. Rock Mech. Eng. 30 (1), 1–22 (In Chinese).

Stead, D., Wolter, A., 2015. A critical review of rock slope failure mechanisms: the importance of structural geology. J. Struct. Geol. 74, 1–23.

The Professional Standards Compilation Group of People's Republic of China, 2007. Design Specification for Slope of Hydropower and Water Conservancy Project. China Electric Power Press (In Chinese).

Tokiwa, T., Tsusaka, K., Ishii, E., Sanada, H., Tominaga, E., Hatsuyama, Y., Funaki, H., 2011. Influence of a fault system on rockmass response to shaft excavation in soft sedimentary rock, Horonobe area, northern Japan. Int. J. Rock Mech. Min. Sci. 48, 773–781.

Um, J., Kulatilake, P.H.S.W., 2001. Kinematic and block theory analyses for shiplock slopes of the Three Gorges Dam Site in China. Geotech. Geol. Eng. 19, 21–42.

Wang, Q., Cui, D., Wang, W., Zhang, S., Liu, J., Shi, Q., 2008. The present vertical crustal movements in part of western Sichuan province. China Sci. D Earth Sci. 38 (5), 598–610 (In Chinese).

Wei, W., Cheng, Y., Li, L., 2009. Three-dimensional slope failure analysis by the strength reduction and limit equilibrium methods. Comput. Geotech. 36 (1), 70–80.

Xu, N., Tang, C., Li, L., Zhou, Z., Sha, C., Liang, Z., Yang, J., 2011. Microseismic monitoring and stability analysis of the left bank slope in Jinping first stage hydropower station in southwestern China. Int. J. Rock Mech. Min. 48, 950–963.

Yao, Y., Zhang, B., Ma, X., Ma, P., 2006. Large-scale hydroelectric projects and mountain development on the upper Yangtze River. Mt. Res. Dev. 26 (2), 109–114.

Zu, Z., Jiang, S., 1988. An inquiry of the time and genesis of Kangding rock complex. J. Earth Sci. Environ. 10 (4), 21–32 (In Chinese).